Preprint Title	Laser-Assisted Synthesis of Colloidal Ni Nanoparticles: Structural and Morphological Analysis
Authors	Monolina Chowdhury, Bibek K. Singh, Sudarshan Vadnala, Archana Tiwari, Ajay Tripathi and Rajesh Rawat
Publication Date	01 Aug. 2024
Article Type	Full Research Paper
Supporting Information File 1	Supplementary Information.docx; 19.0 MB
ORCID® iDs	Bibek K. Singh - https://orcid.org/0009-0006-7433-1971; Archana Tiwari - https://orcid.org/0000-0002-6297-149X; Ajay Tripathi - https://orcid.org/0000-0002-3632-6390; Rajesh Rawat - https://orcid.org/0000-0001-9965-9240

Laser-Assisted Synthesis of Colloidal Ni Nanoparticles: Structural and Morphological Analysis

Monolina Chowdhury[1], Bibek Kumar Singh[2], Sudarshan Vadnala[3], Archana Tiwari[4], Ajay Tripathi[2] and Rajesh Rawat[*1]

Address: [1]Department of Physics, School of Basic Science, SRM University Sikkim, Tadong, 737102, Sikkim, India; [2]Department of Physics, School of Physical Sciences, Sikkim University, 6th mile Samdur, 737102, Sikkim, India; [3]Department of Physics, School of Advanced Sciences, VIT - AP University, Inavolu, Amaravati, Andhra Pradesh, India - 522237 and [4]Department of Physics, Institute of Science, Banaras Hindu University (BHU), Varanasi, 221005, Uttar Pradesh, India

Email: Rajesh Rawat - rajjuu.19@gmail.com

[*] Corresponding author

Abstract

We report on the synthesis of Ni/NiO nanoparticles (NPs) using pulsed laser ablation in liquid (PLAL) technique in deionized water (DI). The laser-generated Ni/NiO NPs in DI show a bimodal size distribution. The structural and morphological analysis using microscopic technique reveal the formation of core-shell structure together with the formation of three distinct features of Ni/NiO nanostructures in DI, nanosheet, hollow and chain-like structures. The formation of a nanosheet-like structure in the colloidal NP solution is attributed to the deformation of the cavitation bubble (CB) and the presence of high pressure at the interface between the bubble and the target during the collapse of CB. The observation of hollow NPs is attributed to the Kirkendall effect and nanochain-like structures due to the post-irradiation effect and laser melting during PLAL. The selected area electron diffraction (SAED) pattern analysis reveals the presence of both Ni and NiO phases indicating the synthesized NPs are polycrystalline. Based on the experimental results, the possible

growth mechanisms for the formation of different structures and morphology of Ni NP in DI during PLAL are discussed.

Keywords

PLAL; Ni/NiO NPs; Structural Analysis; Nanosheet; Hollow NPs; Nano-chain

Introduction

In the field of science and technology, NPs have achieved significant attention due to their unique physico-chemical properties [1]. NPs possess high surface area to volume ratio, which results in surface atom domination over NP properties, exceptional to their bulk counterparts [2-4]. Because of these exceptional properties, NPs are regarded as best suitable candidates for various potential applications such as cancer immunotherapy [5], catalysts [6], optical and electrochemical biosensors [7], environmental remediation [8] and so on. Among all the nanoparticles reported in the literature [9-14], recently Nickel and its oxide (Ni/NiO) NPs have gained appreciable interest in the scientific community because of their combined magnetic and catalytic property [15]. Because of these novel properties, Ni NPs have been extensively used in the application areas of hydrogen evolution reaction (HER) [16], water pollution treatment [17], electrochemical sensor [18], glucose sensing in blood [19] etc. In addition, Ni is more abundant in the earth crust compared to noble metals which makes Ni a preferable candidate compared to noble metals [4]. That is why various research groups have been working on the synthesis of Ni NPs using various techniques. Jaji et al. [15] produced Ni NPs using one-pot solvothermal synthesis technique, which involves chemical reactions at a high temperature and a reaction time. Heilmann et al. [20] reported the synthesis of Ni NPs using a synthetic route, which requires several chemical reactions of Ni acetylacetonate as a precursor, oleylamine as the reducing agent and solvent, dibenzyleether as the co-solvent and trioctylphosphine as the stabilizer. Liu et al. [21] produced shuriken-shaped Ni NPs using thermal decomposition technique. They synthesized face-centred cubic (FCC) Ni nanostructures with an average size of around 150 nm. Zahra et al. [22] synthesized NiO NPs through a sol-gel process facilitated by a polyol medium. In their work they were able to synthesize the FCC

structure of nickel oxide. However, high aggregation of particles resulted in the formation of flakes of irregular sizes and shapes. Using similar technique Shamim et al. [23] reported the synthesis of NiO NPs. Aghaali and Firoozi [24] reported the synthesis of hollow structured Ni NPs via co-solvent ultrasonic spray pyrolysis techniques. Besides various chemical synthesis routes, PLAL is a green, efficient and alternative technique to synthesize ultrapure Ni/NiO NPs and recently it is gaining more interest in the scientific community [1,25-27]. More importantly, the advantage of using PLAL over other techniques is the production of ligand free NPs. In addition, depending on the laser parameters and choice of the solvent, the size, shape, structure and morphology of the NPs can be tuned [9,11,28,29]. To date, several groups have been working on the synthesis and characterization of different properties of Ni NPs produced by PLAL and tried to investigate the parameters on which these properties depend. Mahdi et al. [30] prepared quasi-spherical Ni NPs by laser ablation and studied the dependence of optical absorption of the particles on laser energy and calculated the shift of absorption spectrum with the variation of laser energy. Tailoring particle sizes by varying laser fluence, Mostafa and Mwafy [31] studied the antimicrobial property of Ni/NiO NP. They found that by decreasing the size of NiO crystals, the antibacterial property increases. Bizar et al. [32] produced Au/Ni Oxide nanoalloy and found that addition of Ni increases the conductivity of Au and reduces bandgap energy. Yahaya et al. [33] synthesized Ni NP in different solvents and found that keeping other parameters constant, the productivity of Ni NPs depend on solvent property. They also found unique absorbance spectrum in organic solutions like walnut oil and gum Arabic which indicates the presence of organic functional groups in the colloidal solution. Iacono et al. [34] produced Ni/NiO NPs by PLAL and studied its effects on oxygen evolution reaction (OER). They used Ni/NiO NPs for its catalytic properties and abundance in nature and studied its effectiveness for OER in alkaline media. Subhan et al. [35] reported recently that the morphology and size distribution of produced Ni NPs significantly depend on laser parameters, solvent medium and external field. To study these effects, they used different solvents and applied different external field like electric, magnetic and temperature fields to tailor the production of NPs. Lee et al. [36] also synthesized Ni NPs in different solvents and found that the phases of Ni NPs

strongly depend on solvent properties and cavitation bubble lifetime. They found that while the short lifetime of bubble induces the formation of metastable Ni NP crystals, longer lifetime favors the formation of more stable crystal structures. Rahman and Guisbiers [4] studied the role of laser beam power on the lifetime of cavitation bubble and size distribution of Ni NPs. They found that with the increase in laser beam power, the bubble lifetime decreases and so are the size of the produced NPs. Calderón et al. [37] in their recent work found that laser energy plays excruciating role in the morphology of Ni NPs. At low energy, Ni is found to produce amorphous structures and as energy increases it inclines from polycrystalline to stable crystal structures at high energies.
All these studies discussed above are focused mainly on the synthesis, productivity and characterization of the Ni NPs depending on the laser parameters and the choice of solvent. However, the effect of PLAL dynamics involves during the ablation process resulting in the formation of various nanostructures of Ni particles in the colloid solution was not studied in detail. In this work, an effort has been made to understand the growth mechanism of different nanostructures and morphologies of Ni NPs obtained during PLAL of Ni target in DI. Laser-generated Ni NPs in DI show bimodal size distribution of the particles and the formation of core-shell, nanosheet, hollow and chain-like structure in the sample. The formation of these structures are systematically studied and discussed. It is worth mentioning that the formation of nanosheet-like structure by ablation of Ni target in DI using PLAL technique is the first report to our knowledge. Further, based on the experimental data the possible growth kinetics of formation of these structures are discussed. In addition we have also reported the optical characterization of produced NP colloid.

Materials and Methods

PLAL was performed on a Ni target of dimensions 2 mm × 3 mm × 0.82 mm (99.9% pure), immersed in DI (18 MΩcm at room temperature) by an Nd-YAG Laser (Litron Laser, LYP707-G-10) for a duration of 30 minutes. Prior to the experiment, the target was cleaned thoroughly by ultrasonication in acetone for 30 minutes. Afterward, the target was placed horizontally in the bottom of a glass beaker filled with 8 mL of DI. During the experiment, the liquid layer above the target

surface was kept fixed at 6 mm. The laser beam was focused using a quartz lens of focal length 150 mm onto the target surface, with a measured spot area of 1.5×10^{-3} cm^2. The laser was operated at wavelength of 1064 nm, with pulse duration of 8 ns and repetition rate of 10 Hz and the laser energy was kept at 60 mJ throughout the experiment. The fluence was calculated to be 40 J/cm^2. Ablation rate was found to be 40 μg/s. The target immersed in solvent was continuously stirred with magnetic stirrer at 1020 rpm, to disperse ejected NPs properly in the solvent. To avoid the formation of crater, a translation stage was used to move the target. A total of $4mm \times 4mm$ area was ablated, with a line scan rate of 50 microns per second. To avoid the whirling motion during the process of PLAL, a magnetic bead was kept at the corner of the beaker. The detailed experimental procedure can be found elsewhere [10,11]. After synthesis, the colloidal solution of Ni NPs were collected and subjected to structural and optical studies. The optical study of the sample were carried out by UV-Visible spectrometer using PerkinElmer Lamda 750 in the the range 200-800 nm and Photoluminescence (PL) spectra were recorded using PerkinElmer LS55. The average size, morphology and crystal structure of the laser-generated Ni/NiO NPs were ascertained by TEM and HRTEM using FEI Tecnai G^{2}S-Twin HRTEM working at 200 kV. Estimation of size of the NPs obtained from TEM micrographs was measured using ImageJ software.

Results and Discussion

Structural and Morphological Analysis

To understand the structure and morphology of the Ni NPs, TEM analysis were performed on the produced sample. TEM images of the sample are shown in Fig.1 and Fig.2. The obtained particles are mostly spherical in shape and show bimodal size distribution in the sample. For calculating bigger and smaller particle size, we have considered 84 and 139 particles from different images of the sample respectively. TEM images used for the calculation of bigger and smaller particle size distribution are shown in electronic supplementary information (ESI) Figure S1 (a,b,c and d). The bigger particles (shown in Fig.1(a)) have a median size of 187 nm with standard deviation (SD) of 20 nm and the smaller particles (shown in Fig.1(e) (which is the enlarged image of red solid rect-

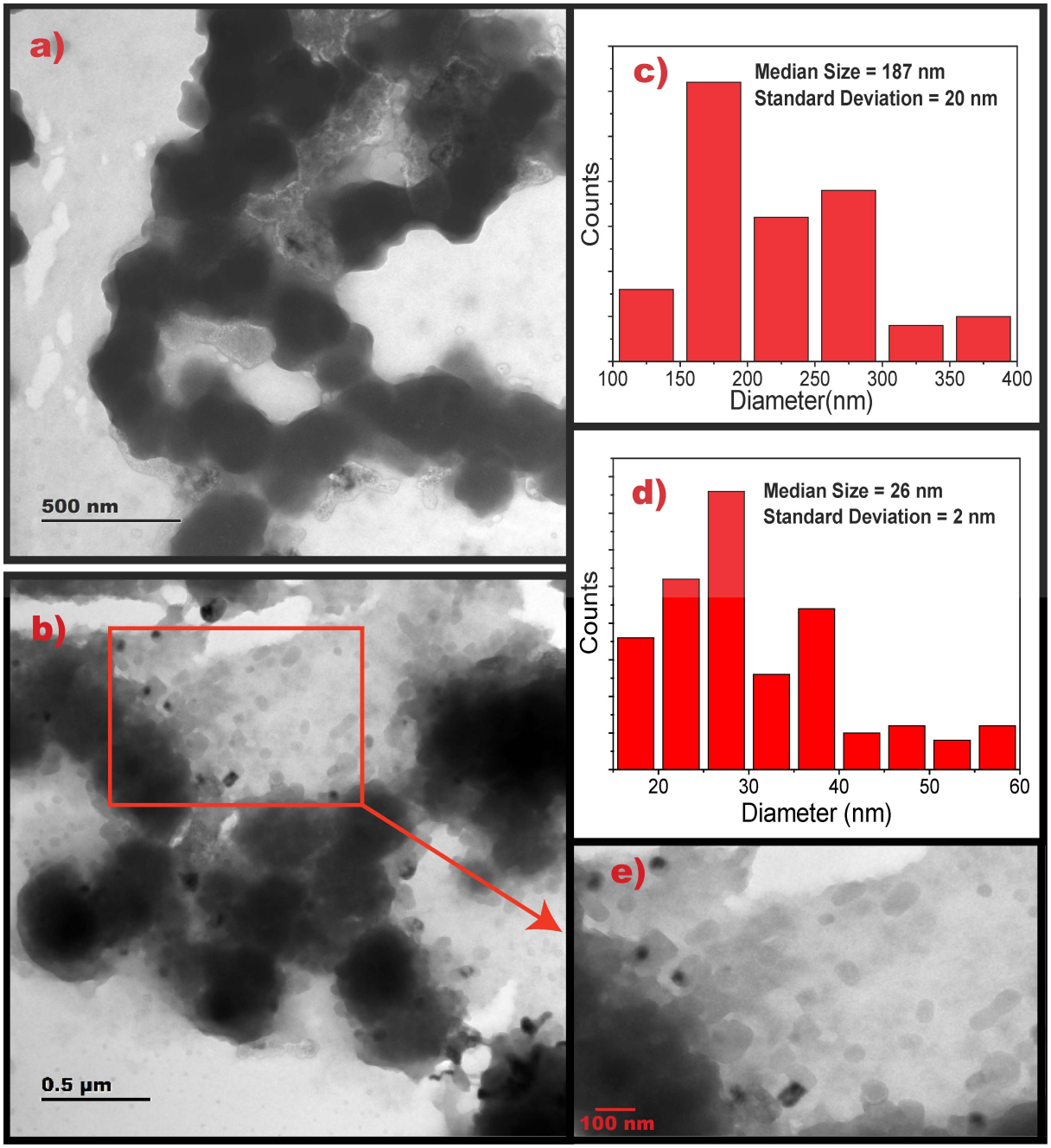

Figure 1: (a) and (b) are the TEM images showing the bimodal size distribution of Ni NPs in DI. For clarity, in (e) the enlarged view of the smaller NPs indicated with a rectangular red region in (b) is shown. In (c) and (d) size distribution histograms of bigger and smaller NPs are shown.

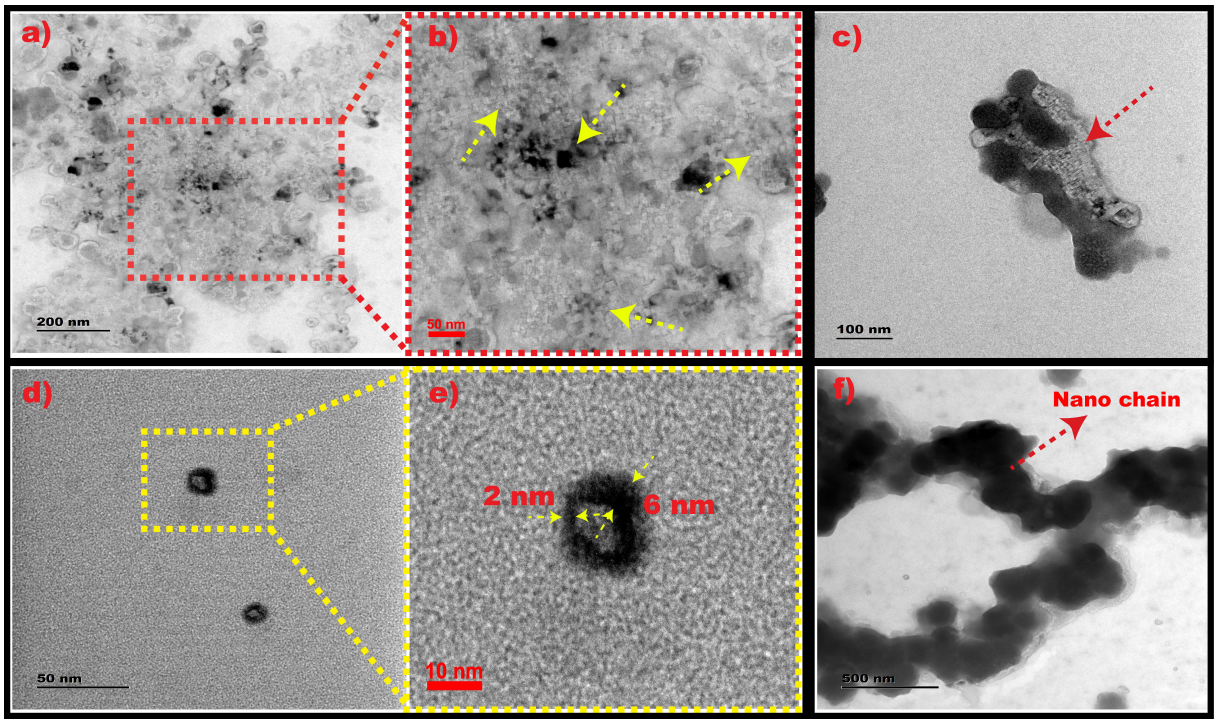

Figure 2: TEM images showing (a) nanosheet-like structure of NPs. For clarity the image of (a) indicated with red dotted rectangular region is zoomed and shown as figure (b), (c) lamellar-like structures (shown with red dotted arrow) of Ni NPs (d) hollow Ni NP. (e) zoomed yellow dotted rectangular region of (d) to show single Hollow NP with non-uniform shell thickness, and (f) Chain-like structure formation of Ni NPs (indicated with red dotted arrow).

angle indicated in Fig.1(b)), have a median size of 26 nm with SD of 2 nm. The size distribution histogram of bigger and smaller particles are shown in Fig.1(c) and Fig.1(d) respectively. The formation of bimodal size distribution of the particles in PLAL is a well known phenomena [38,39]. It is also reported that if no surfactants or stabilizers are used, the produced NPs are inhomogeneous in nature [40]. The production of bigger NPs is attributed to the phenomena of disintegration of hot molten metal surface layer due to continuous evaporation and hydro-static instability. Smaller NPs are generated due to rapid nucleation and growth of the particles inside cavitation bubble from the irradiated zone of the target [38,41]. Upon close examination of TEM images, we observed the formation of core-shell (CS) NPs, along with three distinct structures in the sample: i) nanosheet, ii) Hollow NPs (HNPs), and iii) Chain-like structure, as shown in Fig.2 (b, d and f). The formation of CS NPs can be attributed to the use of DI as solvent. The oxygen present in DI interacted with the metal species during PLAL, resulting in the surface oxidation of the particles to form CS structure. The observation of nanosheet-like structure is shown in Fig.2(b) (indicated with yellow dotted arrow), which is a zoomed-in view of the red rectangular region in Fig.2(a). The formation of these structures is due to the deformation of the cavitation bubble (CB) and the presence of high pressure at the interface between the bubble and the target. The high pressure exerted on the target surface during the collapse of bubble causes the melt on the surface to splash, creating nanosheet-like structures [42-44]. Although sheet-like structures are commonly observed in ultrasound-assisted laser synthesis [45], in our case, they become evident due to minimum crater formation on the surface, as the process constantly exposes new surface for ablation. Upon solidification and aging, these particles get accumulated to form lamellar-like structure as shown in Fig.2(c) with red dotted arrow. Additionally, we observed HNP. In Fig.2(d and e), HNPs with non-uniform shell thickness is shown. The formation of HNPs can be attributed to Kirkendall Effect [46,47]. As mentioned above, due to oxidation, CS structures are formed, initiating the diffusion reaction between the core and the shell. Since the outward diffusion of metal cations is faster than inward diffusion of anions, vacancies form inside the NP to balance the diffusivity gradient. This reaction is particularly evident in smaller-sized NPs where the core completely diffuses into the shell, resulting in the

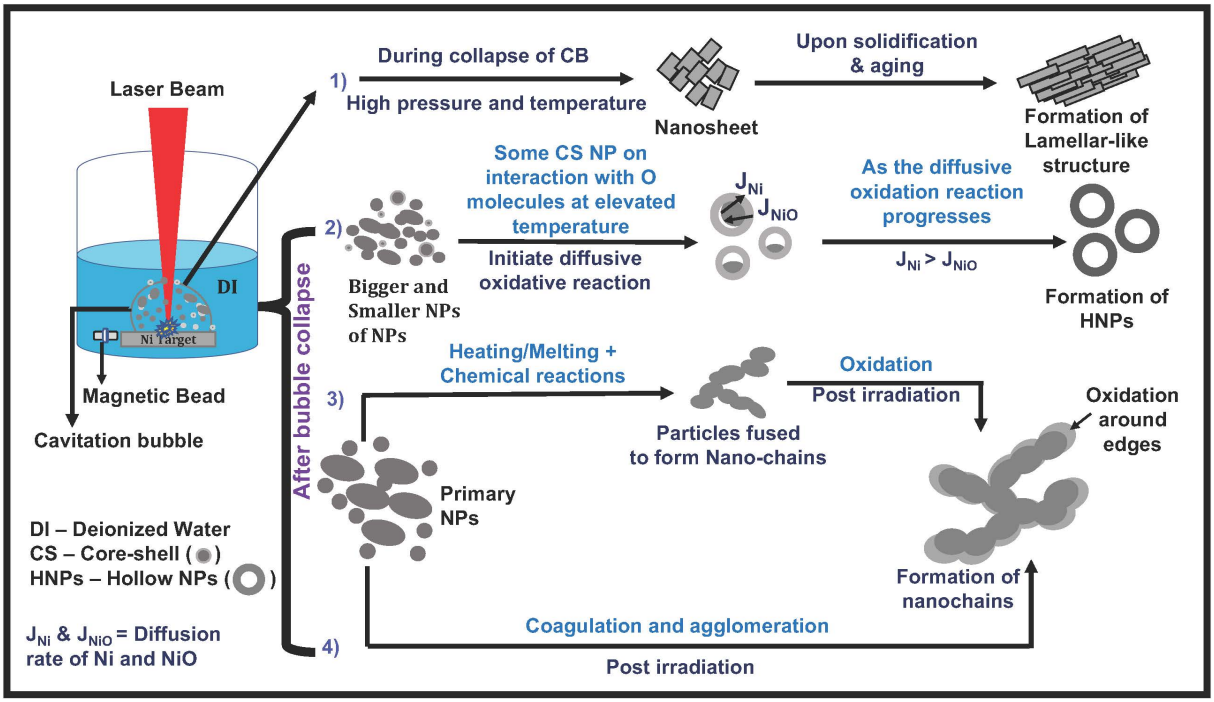

Figure 3: Schematic diagram showing the formation mechanisms of (1) nanosheet-like structure, (2) Hollow NPs, (3) and (4) Nano-chain-like structure during PLAL of Ni target in DI.

formation of voids [48-50]. Given that the self diffusion coefficient of Ni (1.5×10^{-2} cm^2s^{-1}) is higher than that of Oxygen in Ni oxide (1.0×10^{-5} cm^2s^{-1}) [51,52], the outward diffusion of Ni is faster than the inward diffusion of NiO, leading to the formation of HNPs. A similar observation was reported in our previous study on formation of HNP in Cu system [10]. The non-uniform shell thickness can be attributed to the varying rate of diffusion during oxidation process [46,48]. Furthermore, we observed nano-chain structure in the sample (shown in Fig.2(f)) where bigger particles are arranged in a chain-like fashion (indicated with red dotted arrow in Fig.2(f)). The formation of these nano-chain structures can be attributed to two processes during PLAL. Firstly, post laser irradiation, the synthesized larger NPs interact with each other and coagulate to form dimers [53,54]. As the dimer population in the solution grows, they fuse and form chain-like structures [55]. Since Ni is a ferromagnetic material, it agglomerates faster, resulting in the formation of nano-chain structures. Secondly, due to the presence of a whirling process (caused by magnetic beads) during ablation, smaller particles disperse while larger particles remain near the laser beam. Consequently, they undergo further laser treatment, resulting in the melting of the synthesized NPs.

The melting causes these larger particles to fuse together, forming chain-like structure in the sample [56,57], followed by oxidation post-irradiation. The oxidation around the edges of the nano-chain is clearly seen in Fig.2(b). The schematic diagram for the formations of nanosheet, HNPs and nano-chain-like structures are shown in Fig.3(1), (2) and (3, 4) respectively. For confirmation of crystalline structure and the formation of Ni/NiO NP is DI, we have performed SAED measurement on the sample (shown in Fig.4).

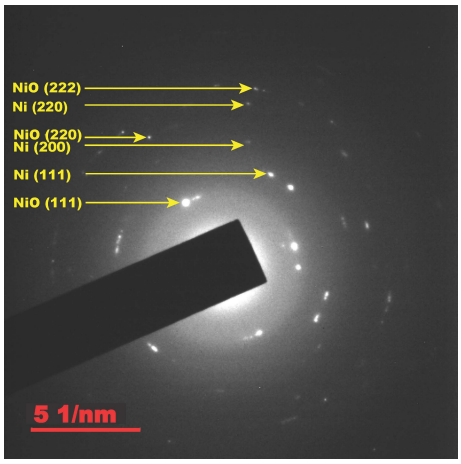

Figure 4: SAED pattern of Ni/NiO NP in DI.

From SAED we observed the formation of Ni/NiO NPs in the sample. The SAED pattern analysis reveals the presence of (111), (200) and (220) crystalline planes of face centered cubic structure of Ni NPs corresponding to the interplanar distance of 2.03 Å, 1.76 Å and 1.24 Å respectively [JCPDS Card No. 01-087-0712;01-078-07533]. In addition, the crystal planes (111), (220) and (222) of NiO phase corresponding to interplanar spacing of 2.42 Å, 1.47 Å and 1.20 Å were also observed [JCPDS Card No. 01-078-0429]. The presence of both Ni/NiO phases indicates that the synthesised NPs are polycrystalline in nature which is in agreement with the obtained TEM result and the absorption spectra analysis of the sample reported in later section.

Optical Analysis

During the PLAL of Ni target in DI for 30 minutes, the colorless ultrapure water is converted into light brownish color indicating the formation of NP in the solution, which is clearly seen in the inset of Fig.5(a). In Fig.5(a) the absorption spectrum of laser-generated colloidal solution of Ni/NiO

NPs is shown. In the figure we have observed two shoulder peaks at 253 nm and 278 nm and a broad peak at ~ 431 nm. The peaks at 253 nm and 278 nm can be attributed to Ni NPs [31,58-60]. The appearance of two peaks corresponding to Ni NP in the sample is due to the presence of heterogeneous size distribution of the particles in the sample. The presence of these peaks is attributed to π - π^* electronic transition in Ni particles [61]. The broad peak at around 431 nm is attributed to NiO NP [62]. The broadening of this peak is due to the oxidation of Ni atoms to form NiO particles. We have also calculated the optical band gap of laser-generated Ni/NiO NPs from the obtained absorption spectra using Tauc relation [11,58] given by:

$$(\alpha h\nu)^n = A(h\nu - E_g)$$

where α is absorption coefficient, $h\nu$ is the photon energy, A is proportionality constant, E_g is band gap energy and n is either 2 or 1/2 for direct or indirect transition respectively. The linear region was obtained by plotting $(\alpha h\nu)^2$ against $h\nu$ indicating direct band gap transition. Fig.5(b) shows the plot of $(\alpha h\nu)^2$ versus $h\nu$ for NiO NP. To plot the graph we have considered the absorption in the range of 250 - 500 nm. Taking extrapolation of the linear region, band gap energy of NiO NPs was calculated to be 4.36 eV, which is larger than the reported value for bulk NiO (3.2 - 4 eV) [63-65]. The higher value of band gap is possibly due to the presence of defects caused by oxidation of NPs. It can be also attributed to the simultaneous presence of Ni and NiO in the synthesized colloidal solution of NPs (shown in Fig.4), which may influence the measured absorption coefficient. Fig.5(c) shows the PL spectra of the synthesized Ni/NiO NPs in DI under the excitation wavelength of 251 nm. On exciting the sample with 251 nm, we observed two emission peaks at 357 nm and 679 nm (as shown in Fig.5(c)). We have also recorded the PL spectra monitoring at excitation wavelengths of 280 nm, 300 nm and 340 nm, and in all the cases emission was observed at 357 nm and 679 nm (data not shown). However the maximum PL intensity of these emission peaks are observed under the excitation wavelength of 251 nm. For this reason the PL spectra recorded under 251 nm excitation wavelength is shown in the study. The presence of these peaks is attributed to the interband transition which have been facilitated because of the presence of defect states in the

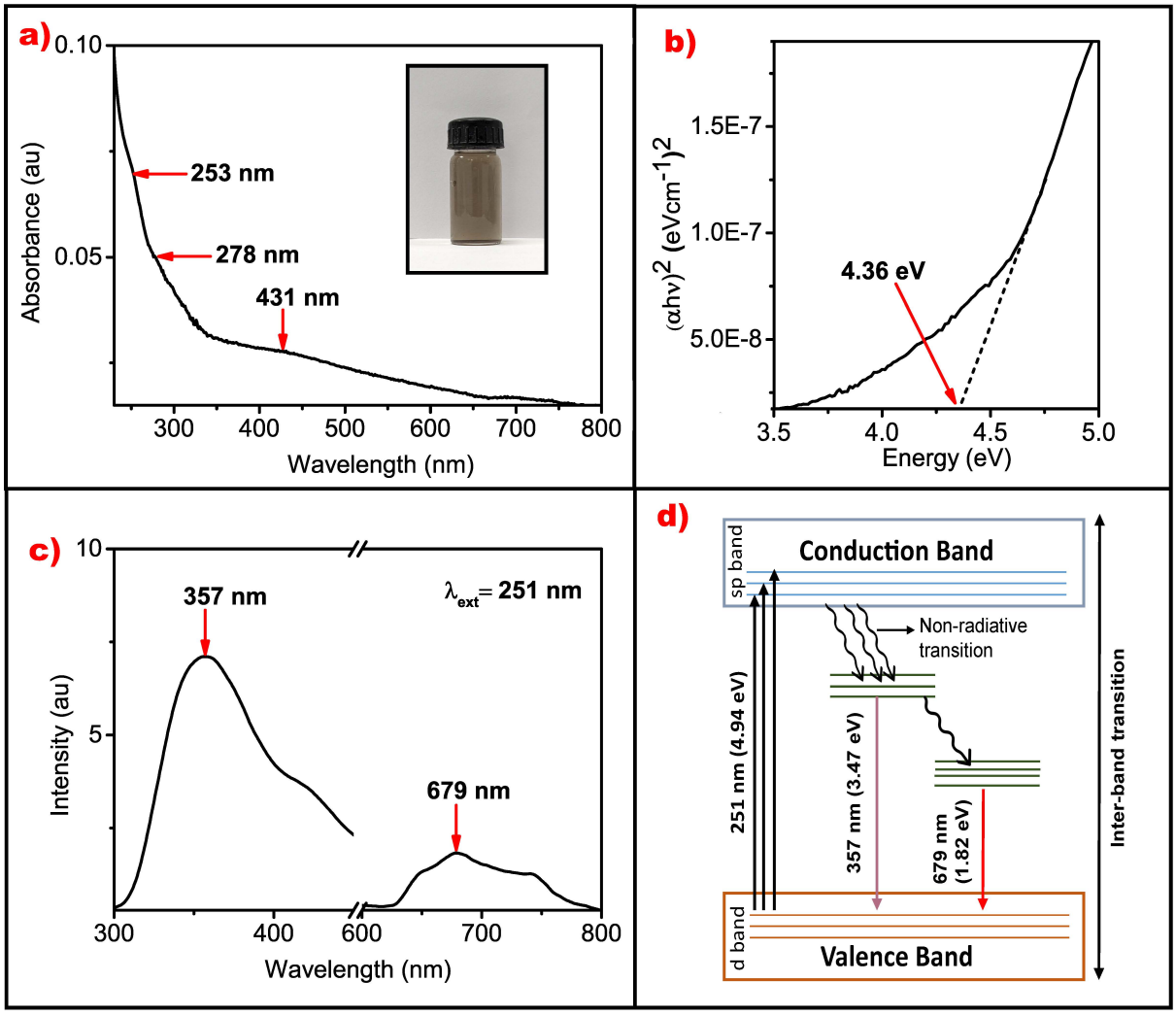

Figure 5: (a) and (b) are the absorption spectrum and $(\alpha h\nu)^2$ versus $h\nu$ plot of Ni/NiO NP in DI. In inset of (a) the colloidal solution of laser-generated Ni NP is shown. (c) PL spectrum of Ni/NiO NP recorded under the 251 nm excitation wavelength and (d) Schematic of energy level diagram of the synthesized NPs.

synthesized NPs. On exciting with 251 nm the high energy levels of sp conduction band gets populated which relaxes to the defects states through non-radiative transition giving an emission around 357 nm (3.47 eV) and 679 nm (1.82 eV). The emission of these peaks lie within the calculated band gap (shown in Fig.5(b)) which further supports the presence of defect states in the sample. The schematic of the energy level diagram is shown in Fig.5(d).

Conclusions

In this study, we systematically investigated the structural and morphological changes in Ni/NiO NPs obtained during PLAL in DI. The Ni/NiO NPs obtained in DI show bimodal size distribution and reveal the formation of different structures and morphologies. The median size of the bigger and smaller particles obtained in DI are 187 ± 20 nm and 26 ± 2 nm. On close observation, the TEM images show formation of CS structure together with the formation of three distinct nanostructures in the sample viz. nanosheet-like structure, hollow and chain-like structures. The formation of CS structured NP in attributed to the use of DI as solvent in which the oxygen present in the DI interact with the metal species during PLAL process resulted in the formation of CS NPs. The observation of nanosheet-like structure in the colloidal NP solution is attributed to the deformation of CB and the presence of high pressure at the interface between bubble an target during the collapse of CB. The observation of HNPs is attributed to the Kirkendall Effect and nano-chain-like structures due to post irradiation effect and laser melting during PLAL. The SAED analysis of the sample reveals the presence of both Ni and NiO phases indicating that the synthesized NPs are polycrystalline in nature which is in agreement with the obtained TEM results. Further, on performing optical characterization of the sample we observed the presence of both Ni and NiO NPs peaks in the laser-generated sample. In the absorption spectrum we have observed two shoulder peaks at 253 nm and 278 nm and a broad peak at around 431 nm. The peaks at 253 nm and 278 nm is attributed to Ni NPs. The appearance of two peaks corresponding to Ni NP in the sample is attributed to the presence of heterogeneous size distribution of the particles in the sample. The

presence of broad peak at 431 nm is attributed to the presence of NiO in the sample. The obtained result are in agreement with the TEM and SEAD analysis.

The present study not only contributes to the understanding of laser-generated Ni/NiO NP behavior in terms of optical, structural and morphological changes in DI but also provides insights in synthesizing and functionality of this nanomaterial for their utilization as a cheaper alternative in the potential applications of nanocatalyst, sensors, water pollution treatment, biomedical and so on.

Acknowledgements

M. Chowdhury and R. Rawat acknowledges the grant from DST-SERB, Govt. of India (File No. EEQ/2022/000191). B.K.Singh acknowledges the grant from the Department of Science and Technology, Govt. of India (Grant No.: DST/INSPIRE Fellowship/2019/IF190981).

References

1. Zhang, D.; Gokce, B.; Barcikowski, S. *Chemical reviews* **2017**, *117* (5), 3990–4103.
2. Geoffrion, L. D.; Guisbiers, G. *Journal of Physics and Chemistry of Solids* **2020**, *140*, 109320.
3. Roduner, E. *Chemical society reviews* **2006**, *35* (7), 583–592.
4. Rahman, A.; Guisbiers, G. *Metals* **2024**, *14* (2), 224.
5. Deng, W.; Shang, H.; Tong, Y.; Liu, X.; Huang, Q.; He, Y.; Wu, J.; Ba, X.; Chen, Z.; Chen, Y. et al. *Journal of Nanobiotechnology* **2024**, *22* (1), 97.
6. Liu, Y.; Tian, X.; Han, Y.-C.; Chen, Y.; Hu, W. *Chinese Journal of Catalysis* **2023**, *48*, 66–89.
7. Beck, F.; Loessl, M.; Baeumner, A. J. *Microchimica Acta* **2023**, *190* (3), 91.
8. Chaudhari, D. S.; Upadhyay, R. P.; Shinde, G. Y.; Gawande, M. B.; Filip, J.; Varma, R. S.; Zboril, R. *Green Chemistry* **2024**.

9. Amendola, V.; Amans, D.; Ishikawa, Y.; Koshizaki, N.; Scirè, S.; Compagnini, G.; Reichenberger, S.; Barcikowski, S. *Chemistry–A European Journal* **2020**, *26* (42), 9206–9242.

10. Rawat, R.; Tiwari, A.; Arun, N.; Rao, S. N.; Pathak, A.; Rao, S. V.; Tripathi, A. *Applied Physics A* **2020**, *126* (3), 226.

11. Rawat, R.; Tiwari, A.; Arun, N.; Rao, S. N.; Pathak, A. P.; Tripathi, A. *ChemistrySelect* **2019**, *4* (35), 10471–10482.

12. Rawat, R.; Tiwari, A.; Vendamani, V.; Pathak, A.; Rao, S. V.; Tripathi, A. *Optical Materials* **2018**, *75*, 350–356.

13. Coviello, V.; Forrer, D.; Canton, P.; Amendola, V. *Nanoscale* **2024**.

14. Lévy, A.; de Anda Villa, M.; Laurens, G.; Blanchet, V.; Bozek, J.; Gaudin, J.; Lamour, E.; Macé, S.; Mignon, P.; Milosavljevic, A. R. et al. *Langmuir* **2021**, *37* (19), 5783–5794.

15. Jaji, N.-D.; Lee, H. L.; Hussin, M. H.; Akil, H. M.; Zakaria, M. R.; Othman, M. B. H. *Nanotechnology reviews* **2020**, *9* (1), 1456–1480.

16. Wang, L.; Li, Y.; Xia, M.; Li, Z.; Chen, Z.; Ma, Z.; Qin, X.; Shao, G. *Journal of Power Sources* **2017**, *347*, 220–228.

17. Garavand, K.; Mosivand, S. *Applied Physics A* **2021**, *127* (1), 73.

18. Neiva, E. G.; Oliveira, M. M.; Marcolino Jr, L. H.; Zarbin, A. J. *Journal of colloid and interface science* **2016**, *468*, 34–41.

19. Jia, H.; Shang, N.; Feng, Y.; Ye, H.; Zhao, J.; Wang, H.; Wang, C.; Zhang, Y. *Journal of Colloid and Interface Science* **2021**, *583*, 310–320.

20. Heilmann, M.; Kulla, H.; Prinz, C.; Bienert, R.; Reinholz, U.; Guilherme Buzanich, A.; Emmerling, F. *Nanomaterials* **2020**, *10* (4), 713.

21. Liu, S.; Mei, J.; Zhang, C.; Zhang, J.; Shi, R. *Journal of Materials Science & Technology* **2018**, *34* (5), 836–841.

22. Zahra, S.; Shahid, W.; Amin, C. A.; Zahra, S.; Kanwal, B. *BMC chemistry* **2022**, *16* (1), 105.

23. Shamim, A.; Ahmad, Z.; Mahmood, S.; Ali, U.; Mahmood, T.; Nizami, Z. A. *Open Journal of Chemistry* **2019**, *2* (1), 16–20.

24. Aghaali, M. H.; Firoozi, S. *Powder technology* **2019**, *356*, 119–128.

25. Balachandran, A.; Sreenilayam, S. P.; Madanan, K.; Thomas, S.; Brabazon, D. *Results in Engineering* **2022**, *16*, 100646.

26. Fazio, E.; Gökce, B.; De Giacomo, A.; Meneghetti, M.; Compagnini, G.; Tommasini, M.; Waag, F.; Lucotti, A.; Zanchi, C. G.; Ossi, P. M. et al. *Nanomaterials* **2020**, *10* (11), 2317.

27. Dell'Aglio, M.; Gaudiuso, R.; De Pascale, O.; De Giacomo, A. *Applied Surface Science* **2015**, *348*, 4–9.

28. Kalus, M.-R.; Barcikowski, S.; Goekce, B. *Chemistry–A European Journal* **2021**, *27* (19), 5978–5991.

29. Kanitz, A.; Kalus, M.; Gurevich, E.; Ostendorf, A.; Barcikowski, S.; Amans, D. *Plasma Sources Science and Technology* **2019**, *28* (10), 103001.

30. Mahdi, R. O.; Hadi, A. A.; Taha, J. M.; Khashan, K. S. Preparation of nickel oxide nanoparticles prepared by laser ablation in water. In *AIP Conference Proceedings*; 2020.

31. Mostafa, A. M.; Mwafy, E. A. *Environmental Nanotechnology, Monitoring & Management* **2020**, *14*, 100382.

32. Bizar, P.; Dorranian, D.; Rasouli, M. *Optical Materials* **2024**, *151*, 115403.

33. Yahaya, N. I. S. B.; Sapian, N. I. H. B.; Duralim, M. B.; Abd Aziz, M. S. B.; binti Alias, S. S.; Husein, N. A. B. et al. Synthesis of nickel nanoparticles by pulsed laser ablation in different liquid media. In *Journal of Physics: Conference Series*; 2023; p 012006.

34. Iacono, V.; Mirabella, S.; Ruffino, F. *physica status solidi (b)* **2023**, *260* (10), 2200590.

35. Subhan, A.; Mourad, A.-H. I.; Al-Douri, Y. *Nanomaterials* **2022**, *12* (13), 2144.

36. Lee, S. J.; Theerthagiri, J.; Choi, M. Y. *Chemical Engineering Journal* **2022**, *427*, 130970.

37. Calderón, V. L.; Ospina, R.; García, F. N. J.; Calderón, C. L. L.; Parra, E. R. *Materials Chemistry and Physics* **2024**, *313*, 128735.

38. Shih, C.-Y.; Streubel, R.; Heberle, J.; Letzel, A.; Shugaev, M. V.; Wu, C.; Schmidt, M.; Gökce, B.; Barcikowski, S.; Zhigilei, L. V. *Nanoscale* **2018**, *10* (15), 6900–6910.

39. Letzel, A.; Gökce, B.; Menzel, A.; Plech, A.; Barcikowski, S. *Applied Surface Science* **2018**, *435*, 743–751.

40. Reichenberger, S.; Marzun, G.; Muhler, M.; Barcikowski, S. *ChemCatChem* **2019**, *11* (18), 4489–4518.

41. Petrov, Y. V.; Khokhlov, V.; Zhakhovsky, V.; Inogamov, N. *Applied Surface Science* **2019**, *492*, 285–297.

42. Dabir-Moghaddam, N.; Liu, Z.; Wu, B. *Journal of Applied Physics* **2017**, *121* (4), year.

43. Azadi, H.; Aghdam, H. D.; Malekfar, R.; Bellah, S. M. *Results in Physics* **2019**, *15*, 102610.

44. Reich, S.; Schönfeld, P.; Wagener, P.; Letzel, A.; Ibrahimkutty, S.; Gökce, B.; Barcikowski, S.; Menzel, A.; dos Santos Rolo, T.; Plech, A. *Journal of colloid and interface science* **2017**, *489*, 106–113.

45. Escobar-Alarcón, L.; Velarde Granados, E.; Solís-Casados, D.; Olea-Mejía, O.; Espinosa-Pesqueira, M.; Haro-Poniatowski, E. *Applied Physics A* **2016**, *122*, 1–7.

328 46. El Mel, A.-A.; Nakamura, R.; Bittencourt, C. *Beilstein journal of nanotechnology* **2015**, *6* (1),
329 1348–1361.

330 47. Zhang, T.; Wang, Z.; Hwang, D. J. *Applied Physics A* **2017**, *123*, 1–7.

331 48. Railsback, J. G.; Johnston-Peck, A. C.; Wang, J.; Tracy, J. B. *ACS nano* **2010**, *4* (4),
332 1913–1920.

333 49. Nakamura, R.; Lee, J.-G.; Mori, H.; Nakajima, H. *Philosophical Magazine* **2008**, *88* (2),
334 257–264.

335 50. Anderson, B. D.; Tracy, J. B. *Nanoscale* **2014**, *6* (21), 12195–12216.

336 51. Atkinson, A.; Taylor, R. *Philosophical Magazine A* **1979**, *39* (5), 581–595.

337 52. O'Keeffe, M.; Moore, W. J. *The Journal of Physical Chemistry* **1961**, *65* (8), 1438–1439.

338 53. Yan, Z.; Bao, R.; Chrisey, D. B. *Physical Chemistry Chemical Physics* **2013**, *15* (9),
339 3052–3056.

340 54. Jendrzej, S.; Gökce, B.; Amendola, V.; Barcikowski, S. *Journal of colloid and interface sci-*
341 *ence* **2016**, *463*, 299–307.

342 55. Mallick, K.; Witcomb, M. J.; Scurrell, M. S. *Materials chemistry and physics* **2005**, *90* (2-3),
343 221–224.

344 56. Jafarkhani, P.; Torkamany, M.; Dadras, S.; Chehrghani, A.; Sabbaghzadeh, J. *Nanotechnology*
345 **2011**, *22* (23), 235703.

346 57. Vendamani, V.; Tripathi, A.; Pathak, A. P.; Rao, S. V.; Tiwari, A. *Materials Letters* **2017**, *192*,
347 29–32.

348 58. Gondal, M.; Saleh, T. A.; Drmosh, Q. *Applied Surface Science* **2012**, *258* (18), 6982–6986.

349 59. Sudhasree, S.; Shakila Banu, A.; Brindha, P.; Kurian, G. A. *Toxicological & Environmental*
350 *Chemistry* **2014**, *96* (5), 743–754.

60. Safa, M.; Dorranian, D.; Masoudi, A.; Matin, L. F. *Applied Physics A* **2019**, *125*, 1–9.

61. Nouneh, K.; Oyama, M.; Diaz, R.; Abd-Lefdil, M.; Kityk, I.; Bousmina, M. *Journal of Alloys and Compounds* **2011**, *509* (19), 5882–5886.

62. Abdelhalim, M. A. K.; Mady, M. M.; Ghannam, M. M. *J Nanomed Nanotechol* **2012**, *3* (3), 178–194.

63. Kamakura, N.; Takata, Y.; Tokushima, T.; Harada, Y.; Chainani, A.; Kobayashi, K.; Shin, S. *Physical Review B* **2006**, *74* (4), 045127.

64. Al-Ariki, S.; Yahya, N. A.; Al-A'nsi, S. A.; Jumali, M. H.; Jannah, A.; Abd-Shukor, R. *Scientific Reports* **2021**, *11* (1), 11948.

65. Sasi, B.; Gopchandran, K. *Nanotechnology* **2007**, *18* (11), 115613.